INTERPLAY OF CORRELATIONS AND FLUCTUATIONS IN AU+AU COLLISIONS AT RHIC

MIKHAIL L. KOPYTINE[1] FOR THE STAR COLLABORATION

[1] *Department of Physics, Kent State University, USA*

Dynamic fluctuations in the local density of non-identified hadron tracks reconstructed in the STAR TPC are studied using the discrete wavelet transform power spectrum technique which involves mixed event reference sample comparison. The two-dimensional event-by-event analysis is performed in pseudo-rapidity η and azimuthal angle ϕ. HIJING simulations indicate that jets and mini-jets result in signals, visible without high p_T selection, when the dynamic texture analysis is applied. Scanning a broad range of event multiplicities, we study the dependence of the signals on the initial conditions. Event structures are studied separately with positive and negative tracks, as well as both charges. A change of regime is observed in AuAu collisions at $\sqrt{S_{NN}} = 130$ GeV as event multiplicity is increased: a long range η correlation (or suppressed fluctuation vis-a-vis mixed events) is seen in same charge data. This effect is qualitatively similar to one of the predicted manifestations of the Color Glass Condensate.

1 Introduction

Bulk properties of strongly interacting matter under extreme conditions are the focus of the on-going RHIC program. Deconfinement and chiral symmetry restoration[1] are expected to take place in collisions of ultra-relativistic nuclei. Because these phase transitions are multiparticle phenomena, a promising, albeit challenging, approach is the study of dynamics of large groups of final state particles. The dynamics shows itself in the correlations and fluctuations (texture) on a variety of distance scales in momentum space.

The multi-resolution dynamic texture approach (applied for the first time[2] at SPS) uses discrete wavelet transform [3](DWT) to extract such information. At present stage, the information is extracted in a comprehensive way, without any built-in assumptions or filters. Mixed events are used as a reference for comparison in search for dynamic effects. Event generators are used to "train intuition" in recognizing manifestations of familiar physics (such as elliptic flow or jets) in the analysis output, as well as to quantify sensitivity to the effects yet unidentified, such as critical fluctuations or clustering of new phase at hadronization.

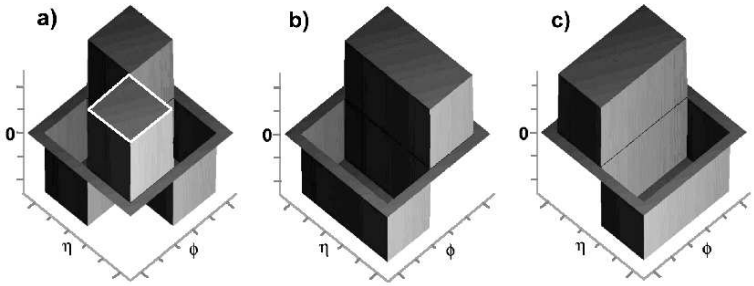

Figure 1: Haar wavelet basis in two dimensions. The three modes of directional sensitivity are: a) diagonal b) azimuthal c) pseudo-rapidity. For the finest scale used, the white rectangle drawn "on top" of the function in panel a) would correspond to the smallest acceptance bin (pixel). Every subsequent coarser scale is obtained by expanding the functions of the previous scale by a factor of 2 in both dimensions. (Reproduced from [2]).

2 The STAR experiment

STAR Time Projection Chamber[4](TPC), mounted inside a solenoidal magnet, tracks charged particles within a large acceptance ($|\eta| < 1.3$, $0 < \phi < 2\pi$) and is well suited for event-by-event physics and in-depth studies of event structure. The data being reported are obtained during the first ($\sqrt{S_{NN}} = 130$ GeV) year of RHIC operation. The minimum bias trigger discriminates on a neutral spectator signal in the Zero Degree Calorimeters[5]. By adding a requirement of high charged multiplicity within $|\eta| < 1$ from the scintillating Central Trigger Barrel, one obtains the central trigger. Vertex reconstruction is based on the TPC tracking. Only high quality tracks found to pass within 3 cm of the event vertex are accepted for the texture analysis.

3 Dynamic texture analysis procedure

Discrete wavelets are a set of functions, each having a proper width, or scale, and a proper location so that the function differs from 0 only within that width and around that location. The set of possible scales and locations is discrete. The DWT transforms the collision event in pseudo-rapidity η and azimuthal angle ϕ into a set of two-dimensional functions. The basis functions are defined in the (η, ϕ) space and are orthogonal with respect to scale and location. We accumulate texture information by averaging the power spectra of many events.

The simplest DWT basis is the Haar wavelet, built upon the *scaling function* $g(x) = 1$ for $0 \leq x < 1$ and 0 otherwise. The function

$$f(x) = \{+1 \text{ for } 0 \leq x < \frac{1}{2}; -1 \text{ for } \frac{1}{2} \leq x < 1; 0 \text{ otherwise}\} \tag{1}$$

is the wavelet function.

The experimental acceptance in η,ϕ, and p_T ($|\eta| < 1$, $0 < \phi < 2\pi$)) is partitioned into bins. The η-ϕ partitions are of equal size, whereas in p_T, the binning is exponential when more than one p_T bin is used. In each bin, the number of reconstructed tracks satisfying the quality cuts is counted.

The scaling function of the Haar basis in two dimensions (2D) $G(\phi, \eta) = g(\phi)g(\eta)$ is just a bin's acceptance (modulo units). The wavelet functions F^λ (where the mode of directional sensitivity λ can be azimuthal ϕ, pseudorapidity η, or diagonal $\phi\eta$) are

$$F^{\phi\eta} = f(\phi)f(\eta), \quad F^\phi = f(\phi)g(\eta), \quad F^\eta = g(\phi)f(\eta). \tag{2}$$

We set up a two dimensional (2D) wavelet basis:

$$F^\lambda_{m,i,j}(\phi, \eta) = 2^m F^\lambda(2^m\phi - i, 2^m\eta - j), \tag{3}$$

where m is the integer scale fineness index, and i and j index the positions of bin centers in ϕ and η. Then, $F^\lambda_{m,i,j}$ with integer m, i, and j are known [3] to form a complete orthonormal basis in the space of all *measurable functions* defined on the continuum of real numbers $L^2(\mathbb{R})$. We construct $G_{m,i,j}(\phi, \eta)$ analogously to Eq.3.

Fig. 1 shows the wavelet basis functions F in two dimensions. At first glance it might seem surprising that, unlike the 1D case, both f and g enter the wavelet basis in 2D. Fig. 1 clarifies this: in order to fully encode an arbitrary shape of a measurable 2D function, one considers it as an addition of a change along ϕ ($f(\phi)g(\eta)$, panel (b)), a change along η ($g(\phi)f(\eta)$, panel (c)), and a saddle-point pattern ($f(\phi)f(\eta)$, panel (a)), added with appropriate weight (positive, negative or zero), for a variety of scales. The finest scale available is limited by the two track resolution, and, due to the needs of event mixing, by the number of available events. The coarser scales correspond to successively re-binning the track distribution. The analysis is best visualized by considering the scaling function $G_{m,i,j}(\phi, \eta)$ as binning the track distribution $\rho(\phi, \eta)$ in bins i,j of fineness m, while the set of wavelet functions $F^\lambda_{m,i,j}(\phi, \eta)$ (or, to be exact, the wavelet expansion coefficients $\langle \rho, F^\lambda_{m,i,j} \rangle$) gives the difference distribution

between the data binned with given coarseness and that with binning one step finer. We use WAILI[6] software to obtain the wavelet expansions.

In two dimensions, it is informative to present the three modes of a power spectrum with different directions of sensitivity $P^{\phi\eta}(m)$, $P^{\phi}(m)$, $P^{\eta}(m)$ separately. We define the **power spectrum** as

$$P^{\lambda}(m) = \frac{1}{2^{2m}} \sum_{i,j} \langle \rho, F^{\lambda}_{m,i,j} \rangle^2, \tag{4}$$

where the denominator gives the meaning of spectral density to the observable. So defined, the $P^{\lambda}(m)$ of a random white noise field is independent of m. However, for physical events one finds $P^{\lambda}(m)$ to be dependent on m due to the presence of **static texture** features such as acceptance asymmetries and imperfections (albeit minor in STAR), and non-uniformity of the $dN/\,d\eta$ shape. In order to extract the **dynamic** signal, we use $P^{\lambda}(m)_{true} - P^{\lambda}(m)_{mix}$ where the latter denotes power spectrum obtained from the **mixed events**. The mixed events are composed of the (η, ϕ) pixels of true events, so that a pixel is an acceptance element of the finest scale used in the analysis, and in no mixed event is there more than one pixel from any given true event. The minimum granularity used in the analysis is 16×16 pixels. [1]

Systematic errors can be induced on $P^{\lambda}(m)_{true} - P^{\lambda}(m)_{mix}$ by the process of event mixing. For example, in events with different vertex position along the beam axis, same values of η may correspond to different parts of the TPC with different tracking efficiency. That will fake a dynamic texture effect in η. In order to minimize such errors, events are classified into **event classes** with similar multiplicity and vertex position. Event mixing is done and $P^{\lambda}(m)_{true} - P^{\lambda}(m)_{mix}$ is constructed within such classes. Only events with z vertex lying on the beam axis within 30 cm from the center of the chamber are accepted for analysis. To form event classes, this interval is further subdivided into five bins. We also avoid mixing of events with largely different multiplicity. Therefore, another dimension of the event class definition is that of the multiplicity of quality tracks in the TPC. For central trigger events, the multiplicity range of an event class is typically 25. For small multiplicity events taken with the minimum bias trigger, the multiplicity range per event class is 10 for multiplicities below 90, and 20 in the range between 90 and 150. For larger multiplicities in the minimum bias sample, this multiplicity range was taken to be 50. Events with less than 15 good quality tracks in the fiducial acceptance are ignored.

[1] For a quick reference, here are the scales in η. Scale 1: $\Delta\eta = 1$; scale 2: $\Delta\eta = 1/2$; scale 3: $\Delta\eta = 1/4$ and so on.

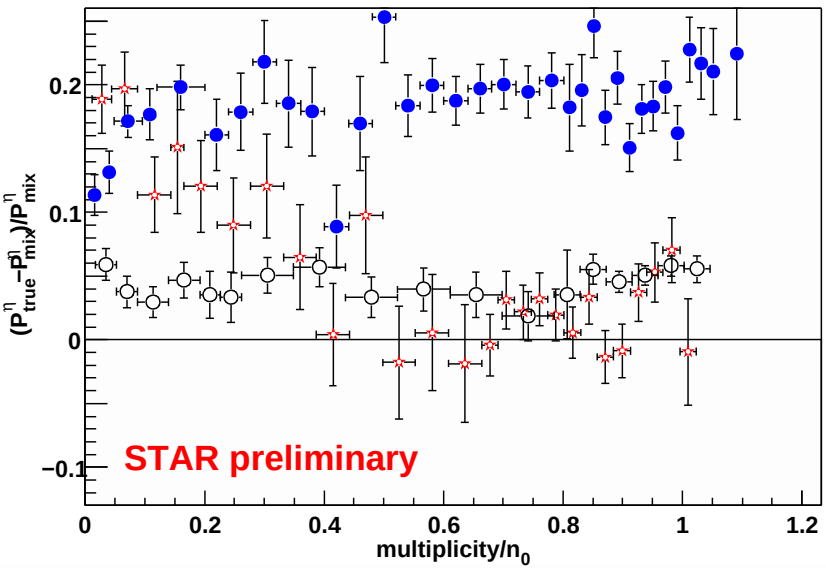

Figure 2: $(P^{\eta}_{true} - P^{\eta}_{mix})/P^{\eta}_{mix}$ (scale 1) in Au Au collisions at $\sqrt{s} = 130$ GeV as a function of normalized multiplicity for **all charged** particles. $\star$ – STAR; $\bullet$ – regular HIJING; $\circ$ – HIJING without jets.

4 Dynamic textures in the STAR data

Elliptic flow is a prominent large scale dynamic texture effect already well measured at RHIC[7]. The DWT approach localizes elliptic flow on scales 2 and, to some degree, 3 of the $P^{\phi}_{true} - P^{\phi}_{mix}$. In this report, we ignore flow and concentrate on the η observables.

Multiplicity scans reveal dependence of the signals on the initial conditions: number of participants and binary collisions and the energy density and size of the interacting system. Such scans as a function of normalized multiplicity [2] are shown in Fig. 2, 3, and 4. The figures show the scale 1 (large scale) observables for tracks of both charges, and for the positive only and the negative only, respectively. The horizontal error bars on the points are formed by multiplicity boundaries of event classes used in the analysis or, when a coarser re-binning of the multiplicity is done on the analyzed data to enhance the presentation, reflect that re-binning. The event mixing is always confined to

[2] To form the normalized multiplicity, the multiplicity n of quality tracks is divided by n_0, where n_0 is such that 99% of minimum bias events have multiplicity of quality tracks less than n_0. The normalized multiplicity depends weakly on the experimental definition of minimum bias and on the track quality cuts.

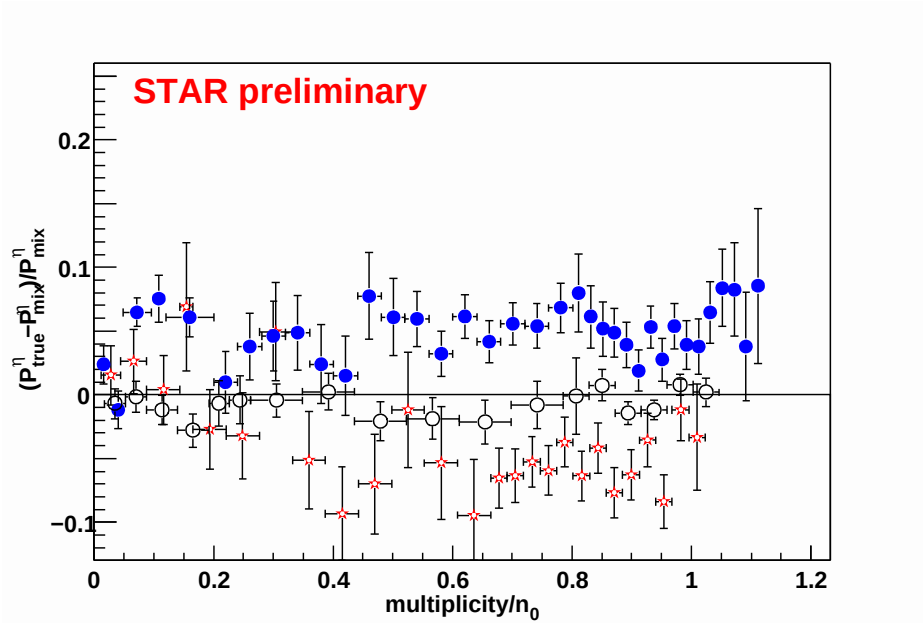

Figure 3: $(P^{\eta}_{true} - P^{\eta}_{mix})/P^{\eta}_{mix}$ (scale 1) in Au+Au collisions at $\sqrt{s} = 130$ GeV as a function of normalized multiplicity for **positively** charged particles. $\star$ – STAR; $\bullet$ – regular HIJING; $\circ$ – HIJING without jets.

the specific multiplicity and z-vertex position class, described in Section 3.

A comparison [3] with HIJING[8] is done in order to understand the effects of energy-momentum conservation, jets and resonances on our measurements. For the regular HIJING and HIJING without jets, the multiplicity dependence is weak or absent. This is understandable given the nature of HIJING as a super-position of binary nucleon-nucleon collisions with no collective effects. The regular HIJING and HIJING without jets show different magnitude of the signal. This underscores the role of jets in creating local density fluctuations (positive dynamic texture) in HIJING. Notice that this result is obtained without imposing a high p_T cut. The experimental data are close to regular HIJING for peripheral events, but their texture becomes suppressed as multiplicity grows.

To understand the nature of this suppression, we look at same charge particles (Fig. 3 and 4). We see that the STAR data are not really intermediate between the regular HIJING and HIJING without jets, but display a more

[3] In the event generator data in the figures, no GEANT and no response simulation is done. Instead, only stable charged particles (e,μ,π,K,p) and their antiparticles from the generator output are considered, provided that they fit into the STAR TPC fiducial η acceptance $|\eta| \leq 1$. Momentum resolution and p_T acceptance are not simulated.

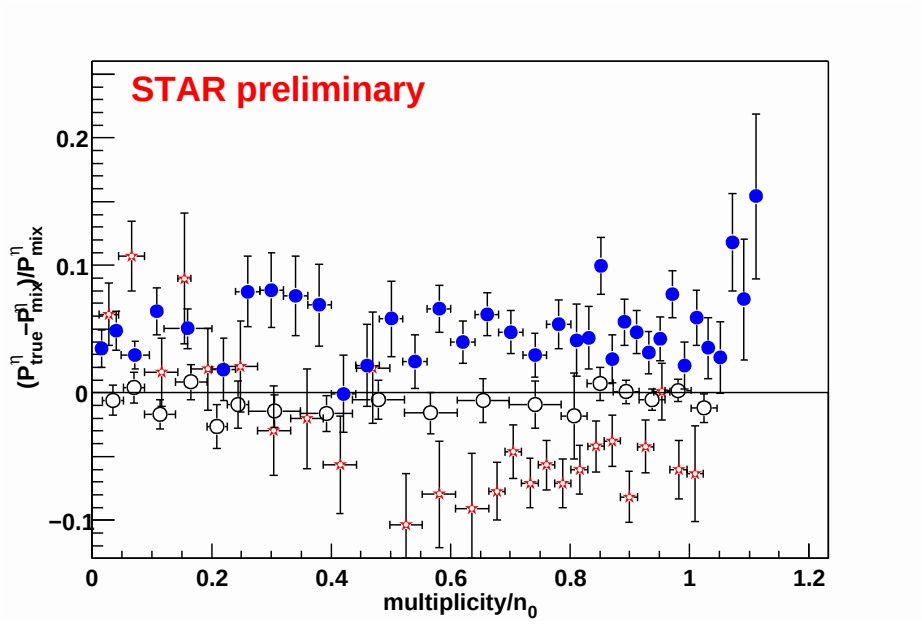

Figure 4: $(P^{\eta}_{true} - P^{\eta}_{mix})/P^{\eta}_{mix}$ (scale 1) in Au+Au collisions at $\sqrt{s} = 130GeV$ as a function of normalized multiplicity for **negatively** charged particles. $\star$ – STAR; $\bullet$ – regular HIJING; $\circ$ – HIJING without jets.

complex behavior. This is seen from the fact that as the multiplicity grows, the dynamic texture becomes negative and stays roughly constant past a transition region which occupies about a half of the multiplicity range, whereas the "no jets" prediction points are consistent with 0 for all multiplicities. How to explain the negative dynamic texture? Recall the definition of the observable (Section 3). At scale 1, we are looking at the fluctuation in same-charge track occupancy between two "pixels", each one unit of η long, located in forward/backward hemispheres around mid-rapidity. The negative $P^{\eta}_{true} - P^{\eta}_{mix}$ means that in the mixed events, this occupancy fluctuation is stronger, i.e. a **correlation** takes place in the real events. [4]

[4] This looked very counter-intuitive to us at first – indeed, the events are composed out of positive and negative charge sub-events. If the positive sub-event shows reduced (negative) fluctuations, and so does the negative sub-event, how can the fluctuation measure for the combined event be above zero ? To ensure that the "balance" is kept, we construct and measure 0 from ρ and ρ_{mix} for positive and negative tracks. In the following, the $\langle \rho | F \rangle$ notation denotes coefficients in the expansion of an individual event track density ρ into wavelet basis F. For simplicity, we omit the indices. We sum over locations but not over the scale index. Averaging over many events is assumed everywhere.

$$\langle \rho^{+} + \rho^{-} | F \rangle^2 - \langle \rho^{+}_{mix} + \rho^{-}_{mix} | F \rangle^2 =$$

The tracking conditions in the chamber are different at high and low multiplicities, and the effect of that on the measurements in question needs to be understood. We do this by processing HIJING events through full GEANT and response simulation, and applying the actual experimental reconstruction to those events. Such processing (done for a smaller number of high multiplicity HIJING events than is shown in the figures) reveals no significant difference for the reported observable.

Thus, we are looking at an interplay of fluctuation and correlation effects, neither of which is trivial, as a function of initial conditions. The signals become weaker for finer scales. At this point one can only speculate about the nature of the correlation effect in central events, but the HIJING simulation indicates that jet quenching (or even total disappearance of jets) does not account for the **negative** $P_{true} - P_{mix}$, even though it may be a prerequisite for its observation, given that jets work to create a **positive** texture. What about Bose-Einstein correlation? In the simulations, its effect can not be introduced into the multiparticle distributions event-by-event from the first principles, and in HIJING it is not considered at all. Low values of Q_{inv} (< 50 MeV[9]), typical for both Bose-Einstein and Coulomb effects, make it unlikely for these effects to be responsible for correlations with characteristic $\Delta\eta \approx 1$.

Longitudinal expansion maps rapidity differences onto time differences; the features characterized by larger rapidity differences must be formed early. In the Color Glass Condensate picture, multiplicity fluctuations in different rapidity windows are predicted to be correlated for large $(1/\alpha_S)$ rapidity intervals[10]. This is seen as a consequence of the classical coherence of the gluon field. Such or a qualitatively similar effect is indeed required to explain the data.

$$\langle\rho^+|F\rangle^2 + \langle\rho^-|F\rangle^2 + 2\langle\rho^+|F\rangle\langle\rho^-|F\rangle - \langle\rho^+_{mix}|F\rangle^2 - \langle\rho^-_{mix}|F\rangle^2 - 2\langle\rho^+_{mix}|F\rangle\langle\rho^-_{mix}|F\rangle \quad (5)$$

We measure independently $\langle\rho^+|F\rangle^2 - \langle\rho^+_{mix}|F\rangle^2$ (Fig.3, modulo normalization) and $\langle\rho^-|F\rangle^2 - \langle\rho^-_{mix}|F\rangle^2$ (Fig.4, modulo normalization). In order to test that Eq.5 holds, we need to obtain the correlation terms between the opposite charges $\langle\rho^+|F\rangle\langle\rho^-|F\rangle$ and $\langle\rho^+_{mix}|F\rangle\langle\rho^-_{mix}|F\rangle$. This can be done by comparing power spectra of images filled with equal weights for positive and negative particles, and of those where negative particles are entered with a negative weight:

$$\langle\rho^+ + \rho^-|F\rangle^2 - \langle\rho^+ - \rho^-|F\rangle^2 = 4\langle\rho^+|F\rangle\langle\rho^-|F\rangle, \quad (6)$$

which is true for ρ_{mix} as well. With this input, validity of Eq.5 has been established and the "paradox" presented above resolved: it is the large scale correlation between positive and negative charges that accounts for the "extra" texture when the positive and negative sub-events are combined.

5 Conclusions

The STAR measurements of AuAu data reveal a non-trivial picture of non-statistical correlations and fluctuations which is qualitatively different for peripheral and central collisions. A possible interpretation of the central data is suppression of jets, combined with particle emission correlated over the length of the order of a unit of rapidity.

[1] H. Meyer-Ortmanns, Rev. Mod. Phys. **68**, 473 (1996)

[2] I. Bearden *et al.* [NA44 Collaboration], Phys. Rev. C. 65 (2002) 044903

[3] I. Daubechies, *Ten Lectures on Wavelets* (SIAM, Philadelphia, 1992) and references therein.

[4] K. H. Ackermann *et al.* [STAR Collaboration], Nucl. Phys. A **661**, 681 (1999); Nucl. Phys. A **698**, 408 (2002).

[5] C. Adler, A. Denisov, E. Garcia, M. Murray, H. Strobele and S. White, Nucl. Instrum. Meth. A **470**, 488 (2001)

[6] G. Uytterhoeven *et al.*, WAILI: Wavelets with Integer Lifting. TW Report 262, Department of Computer Science, Katholieke Universiteit Leuven, Belgium, July 1997.

[7] K. H. Ackermann *et al.* [STAR Collaboration], Phys. Rev. Lett. **86**, 402 (2001); C. Adler *et al.* [STAR Collaboration], Phys. Rev. C **66**, 034904 (2002)

[8] X. N. Wang and M. Gyulassy, Phys. Rev. D **44**, 3501 (1991). M. Gyulassy and X. N. Wang, Comput. Phys. Commun. **83**, 307 (1994)

[9] C. Adler *et al.* [STAR Collaboration], Phys. Rev. Lett. **87**, 082301 (2001)

[10] Y. V. Kovchegov, E. Levin and L. D. McLerran, Phys. Rev. C **63**, 024903 (2001). I am grateful to Larry McLerran for informing me about this prediction during the conference.